Stiffness Modulation in a Humanoid Robotic Leg and Knee

Felix Russell[1], Yukio Takeda[2], Petar Kormushev[3], Ravi Vaidyanathan[1], Peter Ellison[4]

***Abstract*—Stiffness modulation in walking is critical to maintain static/dynamic stability as well as to minimize energy consumption and impact damage. However, optimal, or even functional, stiffness parameterization remains unresolved in legged robotics.**

We introduce an architecture for stiffness control utilising a bioinspired robotic limb consisting of a condylar knee joint and leg with antagonistic actuation. The joint replicates elastic ligaments of the human knee providing tuneable compliance for walking. Further, it locks out at maximum extension, providing stability when standing. Compliance and friction losses between joint surfaces are derived as a function of ligament stiffness and length. Experimental studies validate utility through quantification of: 1) hip perturbation response; 2) payload capacity; and 3) static stiffness of the leg mechanism.

Results prove initiation and compliance at lock out can be modulated independently of friction loss by changing ligament elasticity. Furthermore, increasing co-contraction or decreasing joint angle enables increased leg stiffness, which establishes co-contraction is counterbalanced by decreased payload.

Findings have direct application in legged robots and transfemoral prosthetic knees, where biorobotic design could reduce energy expense while improving efficiency and stability. Future targeted impact involves increasing power/weight ratios in walking robots and artificial limbs for increased efficiency and precision in walking control.

***Index Terms*—Prosthetics and Exoskeletons; Compliant Joints and Mechanisms; Humanoid Robot Systems**

I. INTRODUCTION

CONTROLLABLE stiffness in the human leg is vital to optimise energy efficiency and balance in locomotion [1], [2], as well as to reduce joint and limb damage on impact [3], [4]. Achieving some facsimile of natural stiffness control is a longstanding challenge in walking robots, often attempted through implementation of series elastic actuators (SEAs) employing closed loop position feedback to render forces [2]. Rehabilitation aids for walking [5], [6] and robot exoskeletons [7] have drawn on this approach for cybernetic human-robot systems. Real-time implementation, however, requires the inner controller of actuator impedance to run significantly faster than the outer controller setting the desired impedance [8]. Consequently sensing and actuation must function in the order of $1000\,\mathrm{Hz}$ or more [9]. This can enable robotic limit cycle walking with only very small amounts of power consumed and cost of transport comparable to that of humans [10], [11].

In animals, where the transmission rate of sensor data is considered too slow for this type of closed loop impedance control, it is theorised that control of stiffness comes from the co-contraction of antagonistic pairs of muscles [12]. Antagonistic control has been employed in robotic systems [13], [14] and in some humanoid robot designs [15]. [16], [17]. Tödtheide et al. [16], for example, established accurate position control at frequencies of up to $7\,\mathrm{Hz}$ and stiffnesses ranging from $2.75\,\mathrm{Nmrad}^{-1}$ - $0.55\,\mathrm{Nmrad}^{-1}$. These systems draw on pneumatic impedance or torque control with fixed centre of rotation joints. Conversely, this paper explores how human-like geometry and compliance, a critical part of the human leg mechanism, interacts with antagonistic actuation to achieve simpler impedance control.

A. Benefits of the humanoid knee for robotic systems

The human knee facilitates efficient walking, low power stable standing and an ability to perform high load tasks such as stair climb. No single robotic system is yet able to perform in this way [18]. As such, previous work by the authors [19] has developed a mechanical knee joint with a layout replicating the human knee. It contains: springs of adjustable length to represent ligaments attached at points similar to those found in cadaver studies of the human knee; rolling and sliding joint surfaces (condyles) of a shape derived from human bone data; tendon driven actuation from two pneumatic actuators that act as an antagonistic pair, representing the hamstring and quadriceps muscle groups, and a floating patella (knee cap) that directs forces from the quadriceps to the tibial side of the joint.

Like the human knee it locks out compliantly at maximum extension. At these small angles vertical force from the hip and the knee to the foot acts in front of the centre of rotation, causing the joint to further lock without risk of buckling. This is desirable for users of prosthetic knees where stability in standing is critical. A joint with similar shape to the human

Manuscript received: October, 14th, 2020; Revised January, 18th, 2021; Accepted February, 15th, 2021.

This paper was recommended for publication by Pietro Valdastri upon evaluation of the Associate Editor and Reviewers' comments. This work was supported by the UK Engineering and PhysicalSciences Research Council (EPSRC), UK Medical Research Council (MRC) Confidence in Concept (CiC) Scheme, the UK Dementia Reseaarch Institute Care-Research and Technology Centre (DRI-CRT), and Össur Inc.

[1]Biomechatronics laboratory, Department of Mechanical Engineering, Imperial College London, London, SW7 2AZ, UK. felix.russell12@imperial.ac.uk and r.vaidyanathan@imperial.ac.uk

[2]Mechanical Systems Design Laboratory, Tokyo Institute of Technology, i6-9, 2-12-1 Ookayama, Meguro-ku, Tokyo 152-8552 Japan. takeda.y.aa@mech.titech.ac.jp

[3]Robot Intelligence Lab, Dyson School of Design Engineering, Imperial College London, London, UK. p.kormushev@imperial.ac.uk

[4]Dept. of Orthopaedic Surgery, Haukeland University Hospital, Norway. peter.ellison@outlook.com

Digital Object Identifier (DOI): see top of this page.

knee will also be likely to display knee kinematics that are similar to that of the natural knee. This could have applications for prosthetic knees and exoskeletons where a more human-like joint motion could have a more natural feel to the user, improve symmetry and, for exoskeletons, reduce forces at the points of attachment [20].

Studies on our joint and other bicondylar joints have shown that the direct replication of the structure of the human knee in a robotic setting also provides an advantageous relationship between moment arm and angle [21], [22] and that including a patella may improve joint stability [23]. There has been relatively little interest, however, in replicating human knee geometry in order to achieve control of stiffness. This is of particular relevance for prosthetic knees where users typically have the stiffness and damping properties of the joint tuned for safety and comfort [24]. In human knees the cruciate ligaments have a significant effect on knee stiffness [25]. Therefore, there may be a useful ability to tune the passive stiffness properties of the mechanism by adjusting the properties of the springs. Additionally, antagonistic pair control, combined with human like geometry and compliance, may provide a way to perform active control of leg stiffness on demand without the need for fast controller sample rates, as seen in biological systems.

B. Research questions

This paper investigates control of the leg and knee stiffness for applications in robotics. Specifically, it seeks to understand:

1) how the adjustment of bio-inspired ligament-like structures that have been included in the robotic knee could be used to change range of motion, compliance and friction losses in the joint.
2) how the stiffness, maximum payload capacity and perturbation rejection are affected by modifying co-contraction in the antagonistic pair of actuators on the leg, a system similar to that used in biological systems.

The paper describes the methods used to answer both questions before presenting results from each and a discussion.

II. METHODS

The first of the research questions will be answered using a quasi-static computer simulation of the joint. This methods has been chosen because size constraints limit the choice of spring stiffnesses in the current design and an inability to measure contact pressure limits our ability to record frictional losses. The second of these questions will be answered using a robotic model of the joint.

A. Quasi-static simulation

The simulation solves the statically determinate system of forces on the joint (Figure 1) to find F^{Quad} and the normal and tangential components of the tibiofemoral (TF) contact force, $\mathbf{R^{TF}}$ and $\mathbf{F^{TF}}$, given a known set of external forces, joint angle and position of the TF contact point, x_c. To make the system statically determinant no friction is included in the patellofemoral (PF) joint, modelling the patella as a freely rotating cylinder. The equations can be solved for any chosen θ

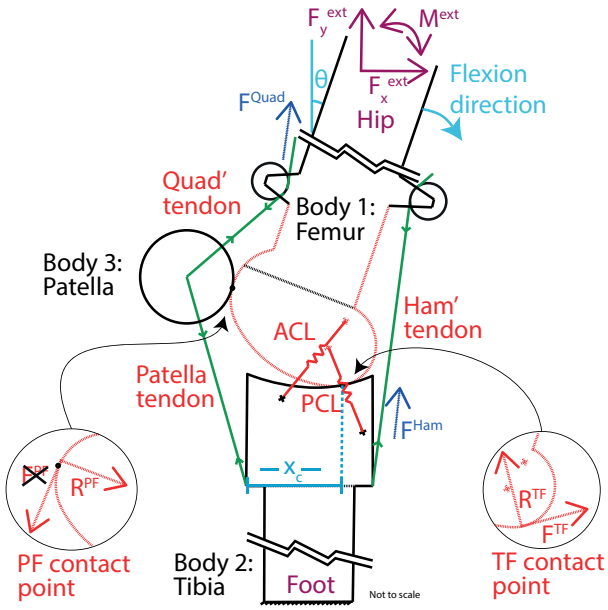

Fig. 1: Simplified model of the joint showing the three rigid bodies considered, the two cruciate ligaments (ACL and PCL), the three tendons linking the three bodies and the two surface contacts. Please note that the patellofemoral (PF) contact is regarded as frictionless. $F^{Patella}$ (not shown) is the tension in the patella tendon.

and x_c. $\mathbf{F^{Ham}}$ is a constant magnitude antagonistic force. The joint is also subject to an external moment and forces on the femur of M^{ext}, F_x^{ext} and F_y^{ext}. For any joint configuration the remaining forces, including the quadriceps, contact and ligament forces, can be calculated.

The ligament forces are found using the known positions of the ligament attachment points combined with their spring rate and slack length. For a given value of θ, the values of x_c are then found that yield the limits of the equilibrium i.e. when $\mu|\mathbf{R^{TF}}| = |\mathbf{F^{TF}}|$ for $\mathbf{F^{TF}}$ pointing both in the anterior and posterior direction. This is done by golden section search across x_c. The range of TF contact points (x_c) that satisfy the equilibrium as a function of joint angle can be found for any given configuration of ligament slack lengths or joint geometry. The two limits of this range will give the relationship between contact point and angle when the joint is moving continuously in each of the flexion or extension directions. When the direction of movement changes from flexion to extension (or vice versa) the contact point will move between the two limits described above. Here $\mu|\mathbf{R^{TF}}| > |\mathbf{F^{TF}}|$ and so no slip between the condyles is assumed. In this region the distance the contact point moves along the tibia and femoral surfaces is the same. These simulation results are validated against experimental results collected as part of the study described in [23].

1) Calculating external forces: The external forces on the system, at every joint angle, θ, are estimated using a simplified static model of the robot leg (Figure 2). Like the robot, the model has one rotational degree of freedom at the foot, a rotational degree of freedom between femur and hip and

a translational degree of freedom between the hip and the global coordinate system. Just for this estimation the knee is approximated as a pin joint. The mass of the tibia, femur (including actuators) and hip and the location of their centres of mass are measured experimentally.

2) Calculating friction losses: TF friction losses are calculated, as a function of ligament slack length, across 20°-110° flexion angles. For a small change in contact point, x_s^{noslip}, the angular movement of the femur that would occur under no slip conditions, $\delta\theta$, is calculated. The change in contact point, δx_s, that is actually observed in the model for that change in angle is then found. The difference gives the relative movement of the surfaces for this small angle change. This is multiplied with the friction force to get the energy loss per radian, $\bar{S}$.

$$\bar{S}(\theta) = F^{TF} \cdot \frac{\delta x_s^{model} - \delta x_s^{noslip}}{\delta\theta} \quad (\mathrm{J/rad}) \qquad (1)$$

B. Robotic testing of antagonist control

Figure 2 shows the robotic knee joint that includes elastic springs that represent the cruciate ligaments, tendon driven pneumatic antagonistic actuation, a patella, joint surface shapes based on human MRI scans and squatting test setup. The bottom of the tibia is able to rotate but not translate as a foot. The hip is fixed to an unactuated sled that constrains the motion to vertical translation above the foot and out of plane rotation of the femur relative to it. The hip height is recorded by an encoder as feedback to the controller. The pneumatic actuators are controlled using Festo proportional-pressure regulators that take an electronic signal to achieve compliant force control in a similar way to human muscles. The tendons are made from ultra high density polyethylene cord with lines of action chosen to match those seen in MRI scans of the knee. More details on how the knee itself was designed to replicate the key features of the human knee are given in previous work by the authors alongside validation of the model by comparison with human kinematics [19], [23]. Position control for the leg sets the quadriceps and hamstring forces and runs at a rate of $150\,\mathrm{Hz}$ in all experiments.

1) Vertical stiffness: For this experiment proportional differential control is implemented on the robotic leg. For each data set the target angle is fixed at a setpoint value, θ_{set}. Steady state error in the system induced by the lack of integral control means that the system instead settles at a larger angle, $\theta_{unloaded}$. Once the system angle has stabilised a mass is added at the hip to apply $41.8\,\mathrm{N}$ vertical force. Once the joint has settled at a new angle, θ_{loaded}, the mass is removed and the system is reset. This is repeated 5 times at $\theta_{set} = [10°, 20°, 30°, 40°, 50°, 60°, 70°, 80°]$ and $A = [10\,\mathrm{N}, 60\,\mathrm{N}, 110\,\mathrm{N}]$ where A is the antagonistic force. The stiffness is then calculated in $\mathrm{Nmm^{-1}}$ as this is a more relevant measure than $\mathrm{Nrad^{-1}}$ for direct application into a robotic system.

2) Payload capacity: A pulley system is used to simulate a payload by applying a negative vertical force at the hip. Figure 3 shows how a winch applies force to the system via a spring balance and large, low stiffness, spring. The spring allows the hip to move with only a small decrease in the amount of downwards force applied.

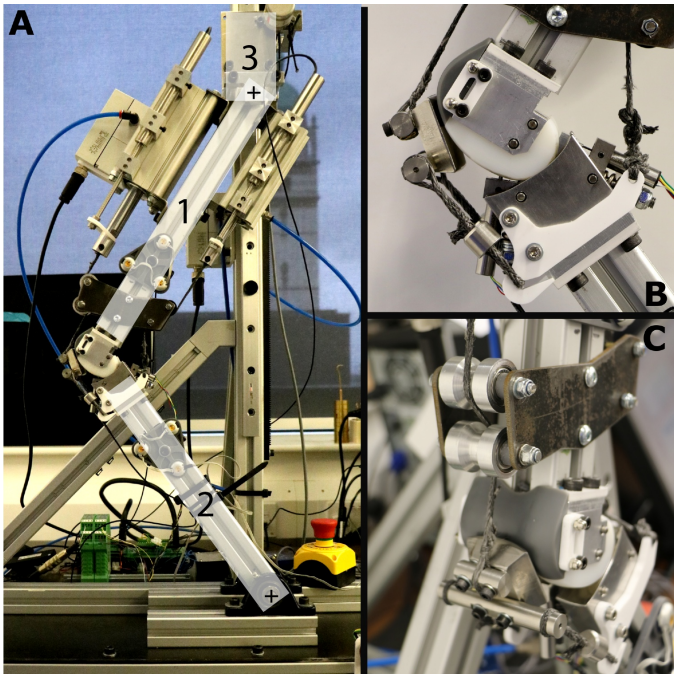

Fig. 2: Robotic leg with human-like knee joint. (A) shows the whole leg system including actuators to represent the quadriceps and hamstrings muscle groups. The labels 1, 2 and 3 indicate the femur, tibia and hip, respectively. (B) shows the joint in profile with the position of the patella and tendons clearly visible. (C) shows a view of the joint from above.

The robot is programmed to perform a $10°\mathrm{s^{-1}}$ ramp to the angle at which the payload capacity is being measured and to maintain that angle. Here integral control is added to remove steady state error. The computer display shows the amount of error between the target angle and the actual angle. The pulley system is slowly tightened to increase the vertical force on the hip while maintaining an error of $0.1 \pm 0.01°$. The value on the spring balance is recorded at the point where the quadriceps actuator becomes saturated ($1680\,\mathrm{N}$). This is done 5 times at each of $\theta = \{100°, 90°, \ldots, 60°, 50°\}$ and $A = [10\,\mathrm{N}, 60\,\mathrm{N}, 110\,\mathrm{N}]$. For $< 50°$ the forces required and therefore energy stored in the spring becomes too high to perform the test safely.

To address this the simulation described in Section II-A is modified to output the maximum payload for a quadriceps force of $1.68\,\mathrm{kN}$, the maximum force the quadriceps actuator can produce. These lines are added to the results to indicate the predicted payload capacity at small angles.

3) Perturbation rejection: A solenoid release mechanism is built to drop a mass of $2.33\,\mathrm{kg}$ onto the hip at a time or joint position set within the computer program. The mass is made up of a cart on the same rail as the hip sled. The height from which the sled drops is adjusted by changing the length of a cord between it and the release. The leg is set to extend at $10°\mathrm{s^{-1}}$ from maximum flexion. The solenoid drops the mass $200\,\mathrm{mm}$ onto the hip as it passes through the set point angle.

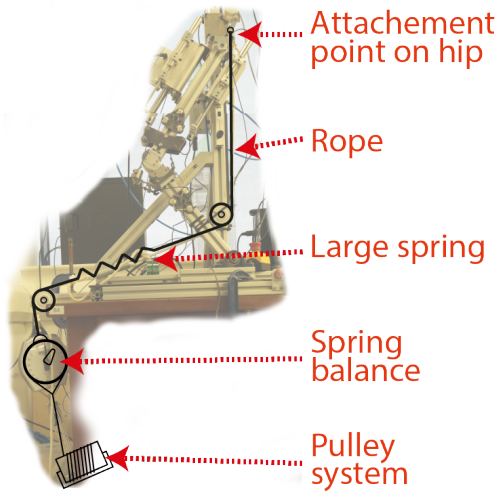

Fig. 3: System for investigating the maximum payload of the knee joint.

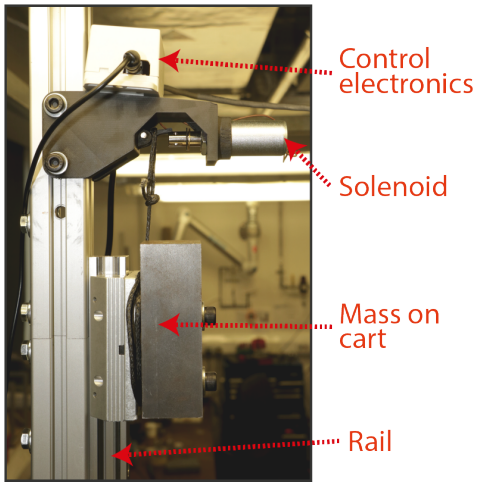

Fig. 4: Quick release system for performing impact tests on the squatting joint.

This makes the energy at impact $E = mgh = 4.57\,\mathrm{J}$. The activation of the solenoid is set $0.2 - 0.3\,\mathrm{s}$ before the set point angle is reached to account for the time taken to fall. The precise value is tuned over a number of test runs for each angle until the timing is accurate to within $1°$. The test is performed at flexion angles $\theta = [30°, 45°, 60°, 75°, 90°]$ and under antagonistic forces of $A = [10\,\mathrm{N}, 60\,\mathrm{N}, 110\,\mathrm{N}]$ with $n = 5$ repeats under each condition.

For each condition the difference between the hip height (measured with an encoder) at impact and the minimum height immediately after impact is recorded. The moment of impact is found by looking for the moment of sudden increase in controller error signal.

The relationships between flexion angle, antagonism and output parameters: stiffness, payload and impact magnitude are tested using multiple regression. The correlation coefficient R is used to quantify the goodness of fit. The presence of a relationship was tested using Fisher's exact test. In all cases $p < 0.05$ is considered to be statistically significant.

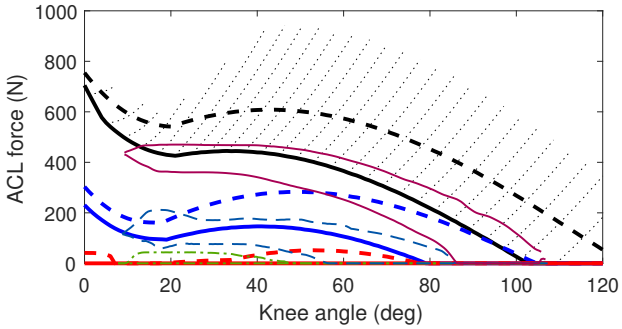

(a) ACL force as a function of ACL length and angle

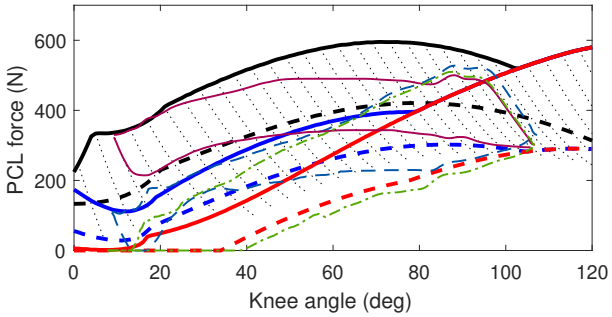

(b) PCL force as a function of ACL length and angle

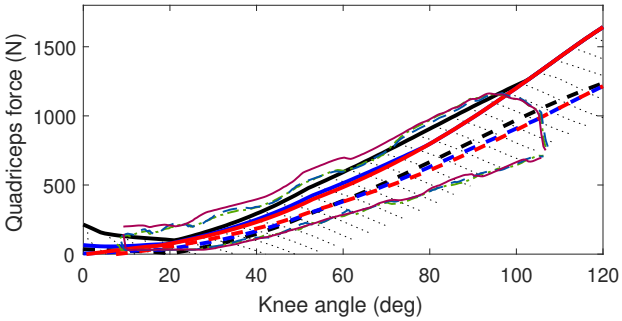

(c) Quadriceps force as a function of ACL length and angle

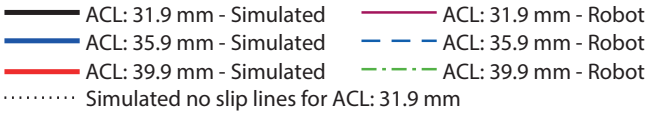

Fig. 5: Comparison of the simulation to the robotic model. The thin lines represent the experimental result, the thick lines the simulation. The no slip lines are shown for only the black configuration to reduce clutter on the plots.

III. RESULTS

A. Simulation

Figures 5a and 5b show that the simulation overestimates the ligament forces compared with those in the robot. However, the overall trends are very similar, the ACL force increases as the joint moves towards maximum extension in both cases and the inverse is true for the PCL. In the ACL, the forces are higher when moving the flexion direction (angle increasing) compared to the inverse for the PCL. Additionally, during

TABLE I: Angle at 200 N quadriceps force (deg)

PCL length ACL length	36.7 mm	38.7 mm	40.7 mm	No PCL
31.9 mm	-0.03	0.70	2.09	2.09
33.9 mm	-4.00	-3.96	-3.78	-3.78
35.9 mm	-8.12	-8.92	-9.22	-9.22
37.9 mm	-12.13	-13.49	-14.12	-14.12
39.9 mm	-15.44	-17.08	-17.87	-17.87
No ACL	-24.84	-29.81	-34.45	N/A

TABLE II: Friction losses in the tibiofemoral joint (J) - Flexion/Extension

PCL length ACL length	36.7 mm	38.7 mm	40.7 mm	No PCL
31.9 mm	7.84/7.11	5.89/5.85	4.24/4.76	2.47/3.78
33.9 mm	7.22/7.20	5.29/5.60	3.65/4.36	2.62/3.57
35.9 mm	6.32/7.40	4.71/5.59	3.34/4.41	2.96/3.78
37.9 mm	5.56/7.54	4.22/5.60	3.34/4.03	3.28/3.80
39.9 mm	5.21/7.49	3.90/5.58	3.42/4.03	3.36/3.80
No ACL	5.37/7.49	3.83/5.58	3.42/4.03	N/A

changes in direction of movement, the paths taken by the metrics of quadriceps force and ligament force lie parallel to the no slip lines in all plots in Figure 5.

1) Range of motion: The range of motion of the joint is tested in simulation by observing the increase in quadriceps force as the flexion angle of the joint approaches and passes into hyperextension ($\theta < 0$). The angle at which the quadriceps force starts to increase and the rate of this increase is measured to indicate respectively the location and stiffness of the end of the range of motion. For this simulation no external forces are applied. Figures 6a and 6b show the effect of changing the ACL slack length and spring stiffness, respectively, on quadriceps force as a function of joint angle. They show that ACL slack length affects the angle at which resistance to hyperextension begins whereas ligament stiffness changes the rate of increase of resistance to hyperextension. Table I summarises this effect of ACL slack length and, for comparison, shows the effect of changing PCL slack length. ACL slack length has the largest effect on range of motion, on average decreasing the $200\,N$ angle by $2.2°$ for every mm of slack length removed compared to $0.7°$ for the same measure for the PCL. The force to hold the joint at $-10°$ is increased by $45.1\,\mathrm{Nmm}^{-1}$ and $9.22\,\mathrm{Nmm}^{-1}$ for shortening the ACL and PCL, respectively.

2) Friction losses: Table II shows the effect that PCL slack lengths have on joint friction at the TF contact under simulated squatting load. The PCL increases friction losses by $0.733\,\mathrm{J}\,(\sigma = 0.192)$ per mm reduction in slack length compared to $0.126\,\mathrm{J}\,(\sigma = 0.158)$ for the ACL. This compares to a mean work done by the quadriceps (across the configurations given below) of $28.0\,\mathrm{J}$ and $-21.0\,\mathrm{J}\,(\sigma = 1.16)$ for extension and flexion, respectively.

B. Experimental results

1) Vertical Stiffness: Figure 7 shows that the vertical stiffness of the hip increases with decreasing flexion angle ($p < 0.001$) and increasing co-contraction ($p < 0.001$) . The lowest stiffness recorded overall is $k = 1.48\,\mathrm{Nmm}^{-1}$ ($\sigma = 0.047\,\mathrm{Nmm}^{-1}$). At the smallest angle tested, $6.4°$, the joint stiffness is $k = 212.8\,\mathrm{Nmm}^{-1}$ ($\sigma = 27.31\,\mathrm{Nmm}^{-1}$) with $10\,\mathrm{N}$ of antagonistic force. This increases to $k = 410.5\,\mathrm{Nmm}^{-1}$ ($\sigma = 63.9\,\mathrm{Nmm}^{-1}$) when the antagonistic force is $110\,N$.

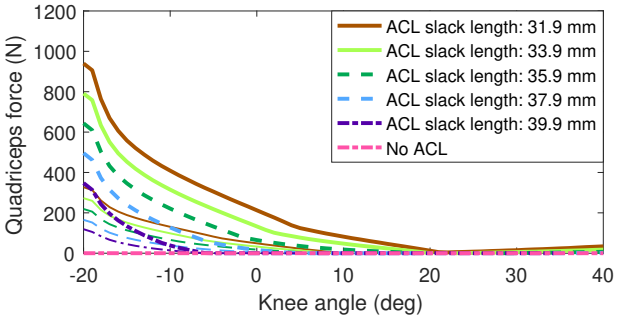

(a) The effect of ACL slack length on quadriceps force.

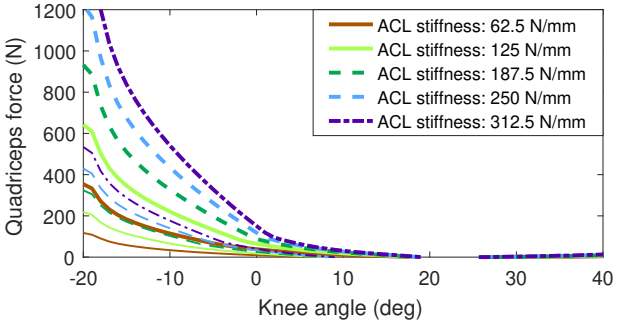

(b) The effect of ACL stiffness on quadriceps force.

Fig. 6: The effect of ACL slack length and stiffness on quadriceps force. The thick and thin lines indicate respectively the forces when moving in the extension and flexion directions.

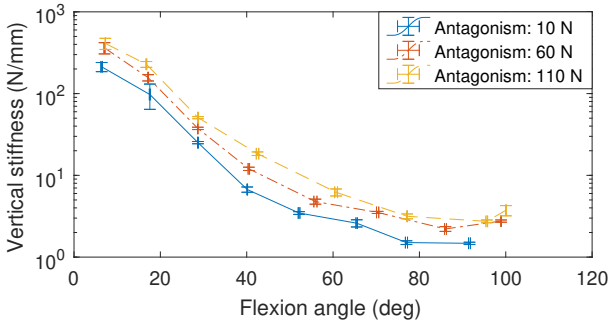

Fig. 7: Vertical stiffness at the hip of the squatting robot leg as a function of angle and antagonistic force. The error bars show standard deviation, σ, ($n = 5$).

2) Payload capacity: Figure 8 shows that the payload capacity of the joint increases with decreasing joint angle ($p < 0.001$) and decreasing co-contraction ($p < 0.001$). At a large flexion angle of $90°$ the joint can support $62.8\,\mathrm{N}\,(\sigma = 7.76)$ to $36.79\,\mathrm{N}\,(\sigma = 6.94)$ when co-contraction from the hamstrings is $10\,\mathrm{N}$ and $110\,\mathrm{N}$, respectively. At $20°$ the model predicts that the joint can raise $46.1\,\mathrm{kN}$ to $44.5\,\mathrm{kN}$ under the same range of antagonistic loads. This does not take into account possible failure of the joint elements under these higher loads.

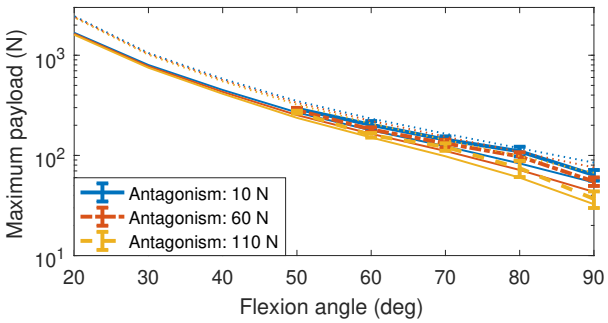

Fig. 8: The maximum vertical payload that can be supported by the leg system. Thick lines with error bars are experimental results with standard deviations ($n = 5$). Thin lines are from the simulation. The dotted line indicates the predicted maximum force the joint can sustain without the hip dropping. The solid line indicates the maximum force the joint can lift.

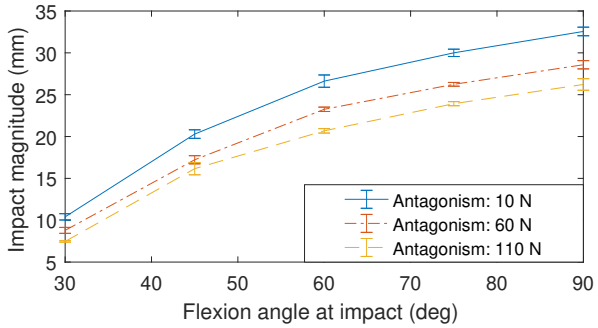

Fig. 9: Robotic results that show the magnitude of the impact of dropping a mass of 2.33 kg from a height of 200 mm. Recorded as a function of joint angle and antagonistic force. Error bars show ± one standard deviation, σ, ($n = 5$).

3) Perturbation rejection: Figure 9 shows that increasing co-contraction, in this case from the hamstrings actuator, decreases the magnitude of the impact response ($p < 0.001$), suggesting an increase in the dynamic vertical stiffness at the hip. As joint angle increases the magnitude of the impact response increases, suggesting a reduction in the dynamic stiffness ($p < 0.001$). In all cases the system is able to recover after impact without going into an unstable regime.

In order to more deeply understand what is happening during the impact Figure 10a shows the mean response of the quadriceps force. This is inferred from the pressure at the exit of the pressure regulator, as well as the height of the hip, both as a function of time. The plot shows that there is lag (21 ms at a normalised response of 0.2) between the hip height beginning to change and the quadriceps pressure increasing. For robotic applications, the recovery time from perturbation is critical in addition to the magnitude of response. Comparing Figures 10b and 10c shows that increasing co-contraction has less effect on the speed of recovery than joint angle. On average increasing co-contraction produces a faster recovery but the effect from changing joint angle is more pronounced, reducing the time taken from 0.27 s to 0.14 s to return to 0 mm

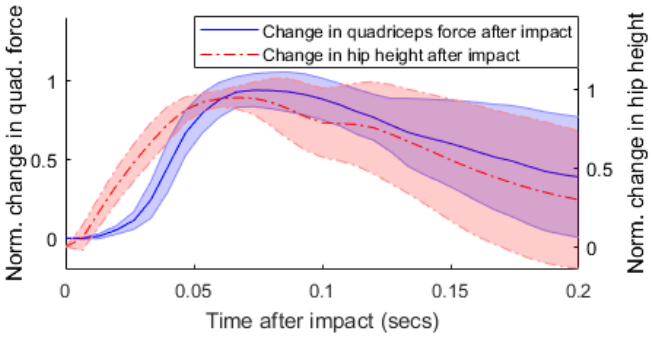

(a) Average response at the hip and of the quadriceps force after impact.

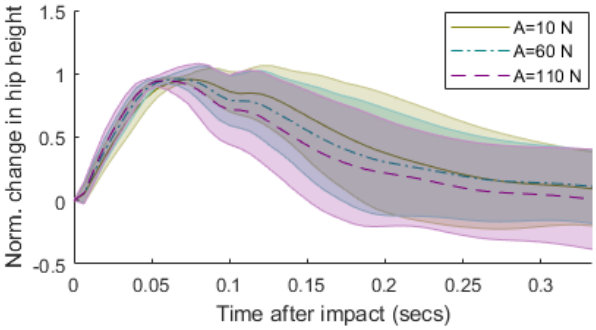

(b) Average response at the hip after impact as a function of the amount of co-contraction, A.

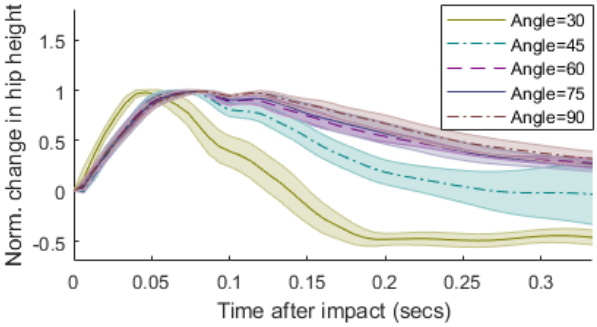

(c) Average response at the hip after impact as a function of the amount of joint flexion angle at impact.

Fig. 10: Average time responses after impact. The shaded area shows standard deviation across ($n = 75, 25, 15$ in (a), (b), (c), respectively). Hip height is normalised by the maximum value in each case.

displacement when the angle is reduced from 45° to 30°. This is confirmed by regression analysis on the normalised displacement, x^* at a time 0.2 s after impact which gives F statistics of 270 ($p < 0.001$) and 10.9 ($p = 0.001$) for angle and antagonism, respectively.

IV. DISCUSSION

A. Ligaments to control joint properties

The simulation shows that the ligament stiffness and length modifies the stiffness of the joint at the limits of extension. This is observed as an increase in the quadriceps force required to extend the joint at this limit. ACL slack length and stiffness

can be selected to control the angle at which this force begins to increase and the stiffness (rate) of the increase. Equally, by tuning PCL length the friction in the joint can be adjusted. Current passive prosthetic knees and knee orthotics have their mechanical properties tuned for the user in order to provide appropriate levels of stability [24]. These systems use an arrangement of springs and dampers with morphology that differs greatly from that of the intact limb. Our results show that a joint with geometry inspired by the human knee may be a basis for a novel knee design that maintains the benefits of the human knee mechanism for stability and symmetry (see Section I-A). It also providing the adjustable stiffness and damping properties required by prosthetic knee users. This is achieved through the adjustment of two springs to control range of motion, compliance of the end stop and damping/friction.

B. Quasi-static simulation

The simulation uses a value of the friction coefficient, μ, of 0.15 similar to that between nylon and steel $(0.15 - 0.7)$ [26], [27]. Small adjustments in μ have minimal impact on the results of Figure 5, with the greatest effect altering hysteresis and the absolute magnitude of the friction losses. The relative effects of decreasing PCL length will remain the same.

The trends observed within the simulation and robot are similar for the effect of changing ligament length on quadriceps force (Figure 5c) and ligament forces (Figures 5a and 5b). In simulation, PF friction is neglected in order to make the system statically determinate and the external forces on the joint are produced by a simplified pin jointed model. Nevertheless, the similarity of the data suggests that the simulation is sufficiently accurate to make the predictions described in the relation to the effect on range of motion and friction losses. More accurate modelling and further experimental testing may be required to take the work forward to clinical application.

C. Active control joint stiffness

In humans leg stiffnesses are modified to compensate for external factors such as surface conditions or to modify gait parameters such as stride length or the required frequency of jumping. For hopping, human leg stiffness varies from $14\,\mathrm{Nmm}^{-1}$ and $28\,\mathrm{Nmm}^{-1}$ at knee angles of $28°$-$19°$, respectively, [28] and is modified by muscle co-contraction as well as angle [29]. This compares to $29.7\,\mathrm{Nmm}^{-1}$ and $130.9\,\mathrm{Nmm}^{-1}$ observed at the lowest levels of co-contraction in the robotic joint. For running the stiffness during the toe off phase of gait, which happens at a similar angle to the above, has been observed to range from between $15\,\mathrm{Nmm}^{-1}$ and $52\,\mathrm{Nmm}^{-1}$ and can be increased to increase stride frequency [30].

Further tuning of the actuator sizes may be required in order for the robotic joint to match human leg stiffness exactly. However in both systems changing the level of co-contraction or angle allows joint stiffness to be controlled. For the slowly applied force used in the static stiffness experiment (Figure 7), the stiffness change comes from the mechanics of the joint and the applied control law. The results show that stiffness increases with decreasing joint angle and by increasing co-contraction in the joint. Joint angle and co-contraction both affect the joint's ability to reject perturbation where decreasing angle and increasing co-contraction both decrease the change in height after a vertical impact and decrease the time taken to recover from impact. Other robotic systems demonstrate that this type of passive compliance can reduce force transmission in the instant between impact and the reaction of the control system [3]. Our results show such a lag between the perturbation of hip height and the quadriceps force increasing (Figure 10a). Any increases in joint stiffness with co-contraction comes at a cost of payload capacity (Figure 8). This will set a minimum available amount of co-contraction depending on the required payload and actuator size.

The actuator stiffness before the controller reacts will be controlled by the adiabatic compression of the air. This stiffness is given in Equation 2 where L_0 is the cylinder length just before impact, L is the current length, γ is the ratio of specific heats of air (≈ 1.4), F_0 is the initial actuator force, and r is the mechanical advantage of the actuator.

$$\frac{dM}{d\theta} = r^2\frac{dF}{dL} = -r^2\gamma F_0 L_0^{\gamma} L^{-(\gamma+1)} \approx r^2\gamma\frac{F_0}{L} \qquad (2)$$

Other pneumatic antagonistic control systems use either double acting actuators [16] or non-linear pneumatic muscle actuators (PMAs) [17], [31] with constant mechanical advantage. Conversely the human-like geometry of our joint has complaint elements (tendon and ligaments) built into the joint in addition to the actuators and changing mechanical advantage, r, with angle. Further investigation is required into the cause of the co-contraction stiffness effect in the bio-inspired leg. This is likely to be a combination of: the different amounts that F_0 increases for each actuator in Equation 2; an increase in the ligament forces, including bringing ligaments into tension that would otherwise be slack; increasing contact forces and, therefore, friction in the joint.

Understanding the interaction of these factors is critical for the application of this technology in legged robotic systems. Nevertheless the work here shows that the bicondylar joint, controlled with an antagonistic pair of actuators, can provide control of joint stiffness independently of leg length/angle and, importantly, without the need to increase controller gains. In humans gains are limited by the sample and transmission rates of biological sensors making antagonistic control a key mechanism to change joint stiffness [12]. Equally robotic systems requiring high gains need fast control cycle times that increase the cost of implementation. Our bio-inpired system has a controller running at $150\,\mathrm{Hz}$, slower than the $> 1000\,\mathrm{Hz}$ required in SEA systems [9]. Control of stiffness is critical for efficient gait [1]. Our system, implemented in a walking robot, has the potential to achieve these efficiency benefits even at these low sample rates.

V. CONCLUSION

We introduce a robotic design enabling modulation of stiffness in a bicondylar joint mimicking the geometry of the human knee. The joint locks out compliantly at maximum extension and contains two elastic links that replicate the

function of the human ACL and PCL. We demonstrate that by changing length and stiffness of the ACL spring the angle and stiffness of compliance at lock out can be adjusted. Reducing the length of the PCL further allows joint friction loss to be increased. This has strong implications in design of prosthetic knees for transfemoral amputees where patients often have stiffness and stability needs that demand tuning of springs and dampers at significant expense. Our system achieves similar outcomes through the adjustment of two springs in a simple mechanism while replicating the stability, efficiency and kinematics of the knee.

The robotic experiments demonstrate that the stiffness of the joint and the ability to reject perturbations increases with decreasing joint angle and increasing co-contraction from an antagonistic actuator. In the real world controller gains are often limited, in part, by system sample rates. The bio-inspired system described here demonstrates stiffness control at any leg length/angle despite slow sample rates and without increasing controller gain values. This enables variable stiffness as a practical and achievable outcome in field robotics. It also enables applications for legged robotic systems where leg stiffness is controlled to reduce damage from landing impacts and to increase efficiency of gait.

REFERENCES

[1] C. Hubicki, J. Grimes, M. Jones, D. Renjewski, A. Spröwitz, A. Abate, and J. Hurst, "Atrias: Design and validation of a tether-free 3d-capable spring-mass bipedal robot," *The International Journal of Robotics Research*, vol. 35, no. 12, pp. 1497–1521, 2016.

[2] P. Kormushev, B. Ugurlu, D. G. Caldwell, and N. G. Tsagarakis, "Learning to exploit passive compliance for energy-efficient gait generation on a compliant humanoid," *Autonomous Robots*, vol. 43, no. 1, pp. 79–95, 2019.

[3] H. Dallali, P. Kormushev, N. G. Tsagarakis, and D. G. Caldwell, "Can active impedance protect robots from landing impact?" in *2014 IEEE-RAS International Conference on Humanoid Robots*. IEEE, 2014, pp. 1022–1027.

[4] A. Lees, "Methods of impact absorption when landing from a jump," *Engineering in Medicine*, vol. 10, no. 4, pp. 207–211, 1981.

[5] W. Huo, S. Mohammed, J. Moreno, and Y. Amirat, "Lower limb wearable robots for assistance and rehabilitation: A state of the art," 2014.

[6] P. Cherelle, V. Grosu, P. Beyl, A. Mathys, R. Van Ham, M. Van Damme, B. Vanderborght, and D. Lefeber, "The maccepa actuation system as torque actuator in the gait rehabilitation robot altacro," in *2010 3rd IEEE RAS & EMBS International Conference on Biomedical Robotics and Biomechatronics*. IEEE, 2010, pp. 27–32.

[7] J. E. Pratt, B. T. Krupp, C. J. Morse, and S. H. Collins, "The roboknee: an exoskeleton for enhancing strength and endurance during walking," in *Robotics and Automation, 2004. Proceedings. ICRA'04. 2004 IEEE International Conference on*, vol. 3. IEEE, 2004, pp. 2430–2435.

[8] M. Zinn, B. Roth, O. Khatib, and J. K. Salisbury, "A new actuation approach for human friendly robot design," *The international journal of robotics research*, vol. 23, no. 4-5, pp. 379–398, 2004.

[9] R. Van Ham, B. Vanderborght, M. Van Damme, B. Verrelst, and D. Lefeber, "Maccepa, the mechanically adjustable compliance and controllable equilibrium position actuator: Design and implementation in a biped robot," *Robotics and Autonomous Systems*, vol. 55, no. 10, pp. 761–768, 2007.

[12] N. Hogan, "Adaptive control of mechanical impedance by coactivation of antagonist muscles," *IEEE Transactions on automatic control*, vol. 29, no. 8, pp. 681–690, 1984.

[10] S. H. Collins, M. Wisse, and A. Ruina, "A three-dimensional passive-dynamic walking robot with two legs and knees," *The International Journal of Robotics Research*, vol. 20, no. 7, pp. 607–615, 2001.

[11] P. A. Bhounsule, J. Cortell, A. Grewal, B. Hendriksen, J. D. Karssen, C. Paul, and A. Ruina, "Low-bandwidth reflex-based control for lower power walking: 65 km on a single battery charge," *The International Journal of Robotics Research*, vol. 33, no. 10, pp. 1305–1321, 2014.

[13] S. C. Jacobsen, H. Ko, E. K. Iversen, and C. C. Davis, "Antagonistic control of a tendon driven manipulator," in *Proceedings, 1989 International Conference on Robotics and Automation*. IEEE, 1989, pp. 1334–1339.

[14] S. C. Jacobsen, H. Ko, E. K. Iversen, and C. C. Davis, "Control strategies for tendon-driven manipulators," *IEEE Control Systems Magazine*, vol. 10, no. 2, pp. 23–28, Feb 1990.

[15] V. Potkonjak, B. Svetozarevic, K. Jovanovic, and O. Holland, "The puller-follower control of compliant and noncompliant antagonistic tendon drives in robotic systems," *International Journal of Advanced Robotic Systems*, vol. 8, no. 5, pp. 143–155, 2011.

[16] A. Tödtheide, T. Lilge, and S. Haddadin, "Antagonistic impedance control for pneumatically actuated robot joints," *IEEE Robotics and Automation Letters*, vol. 1, no. 1, pp. 161–168, 2015.

[17] I. Sardellitti, J. Park, D. Shin, and O. Khatib, "Air muscle controller design in the distributed macro-mini (dm 2) actuation approach," in *2007 IEEE/RSJ international conference on intelligent robots and systems*. IEEE, 2007, pp. 1822–1827.

[18] P. A. Bhounsule, J. Cortell, and A. Ruina, "Design and control of ranger: an energy-efficient, dynamic walking robot," in *Proc. CLAWAR*, 2012, pp. 441–448.

[19] F. Russell, R. Vaidyanathan, and P. Ellison, "A kinematic model for the design of a bicondylar mechanical knee," in *2018 7th IEEE International Conference on Biomedical Robotics and Biomechatronics (Biorob)*. IEEE, 2018, pp. 750–755.

[20] D. Zanotto, Y. Akiyama, P. Stegall, and S. K. Agrawal, "Knee joint misalignment in exoskeletons for the lower extremities: Effects on user's gait," *IEEE Transactions on Robotics*, vol. 31, no. 4, pp. 978–987, 2015.

[21] F. Russell, Y. Zhu, W. Hey, R. Vaidyanathan, and P. Ellison, "A biomimicking design for mechanical knee joints," *Bioinspiration & biomimetics*, vol. 13, no. 5, p. 056012, 2018.

[22] A. C. Etoundi, R. Vaidyanathan, and S. C. Burgess, "A bio-inspired condylar hinge joint for mobile robots," in *Intelligent Robots and Systems (IROS), 2011 IEEE/RSJ International Conference on*. IEEE, 2011, pp. 4042–4047.

[23] F. Russell, P. Kormushev, R. Vaidyanathan, and P. Ellison, "The impact of acl laxity on a bicondylar robotic knee and implications in human joint biomechanics," *IEEE Transactions on Biomedical Engineering*, vol. 67, no. 10, pp. 2817–2827, 2020.

[24] H. Herr and A. Wilkenfeld, "User-adaptive control of a magnetorheological prosthetic knee," *Industrial Robot: An International Journal*, 2003.

[25] H. Jonsson, "Knee joint laxity and kinematics after anterior cruciate ligament rupture roentgen stereophotogrammetric and clinical evaluation before and after treatment," *Acta Orthopaedica Scandinavica*, vol. 65, no. sup256, pp. 117–117, 1994.

[26] M. Pascoe and D. Tabor, "The friction and deformation of polymers," *Proceedings of the Royal Society of London. Series A. Mathematical and Physical Sciences*, vol. 235, no. 1201, pp. 210–224, 1956.

[27] R. Steinbuch, "Nylon 6 as a bearing material," *Wear*, vol. 5, no. 6, pp. 458–466, 1962.

[28] C. T. Farley, H. H. Houdijk, C. Van Strien, and M. Louie, "Mechanism of leg stiffness adjustment for hopping on surfaces of different stiffnesses," *Journal of applied physiology*, vol. 85, no. 3, pp. 1044–1055, 1998.

[29] J. Oliver and P. M. Smith, "Neural control of leg stiffness during hopping in boys and men," *Journal of Electromyography and Kinesiology*, vol. 20, no. 5, pp. 973–979, 2010.

[30] C. T. Farley and O. Gonzalez, "Leg stiffness and stride frequency in human running," *Journal of biomechanics*, vol. 29, no. 2, pp. 181–186, 1996.

[31] T. Noritsugu and T. Tanaka, "Application of rubber artificial muscle manipulator as a rehabilitation robot," *IEEE/ASME Transactions On Mechatronics*, vol. 2, no. 4, pp. 259–267, 1997.